Title

Quantitative assessment of renal arterial occlusion in a porcine model using spatial frequency domain imaging.

Journal

Optics Letters, 38(18)

ISSN

0146-9592

Authors

Nadeau, KP
Ponticorvo, A
Lee, HJ
et al.

Publication Date

2013-09-15

DOI

10.1364/ol.38.003566

Quantitative assessment of renal arterial occlusion in a porcine model using spatial frequency domain imaging

K. P. Nadeau,[1] A. Ponticorvo,[1] H. J. Lee,[2] D. Lu,[3] A. J. Durkin,[1] and B. J. Tromberg[1,*]

[1]Laser Microbeam and Medical Program (LAMMP), Beckman Laser Institute, 1002 Health Sciences Road, Irvine, California 92612, USA

[2]Department of Urology, University of California, Irvine, 333 The City Boulevard West, Suite 2100, Orange, California 92868, USA

[3]Department of Pathology, University of California, Irvine, D440 Medical Sciences I, Irvine, California 92697, USA

*Corresponding author: bjtrombe@uci.edu

Received June 11, 2013; accepted July 15, 2013;
posted August 16, 2013 (Doc. ID 192108); published September 6, 2013

We present the results of a feasibility study with spatial frequency domain imaging (SFDI) to produce quantitative measurements of optical property and chromophore concentration maps of three porcine kidneys utilizing a renal occlusion model at the near-infrared wavelengths of 658, 730, and 850 nm. Using SFDI, we examined the dynamics of absolute oxygen saturation (StO_2). The mean StO_2 for the kidneys varied from approximately 60% before occlusion, to 20% during occlusion, to 55% after reperfusion. We also present, for the first time to the best of our knowledge, reduced scattering coefficient (μ_s') maps of the kidney during occlusion. We observed a substantial decrease in the wavelength dependence of scattering (i.e., scattering power) in the three kidneys, with a mean decrease of $18\% \pm 2.6\%$, which is indicative of an increase in scatterer size, and is likely due to tissue changes such as edema that follow from occlusion and inflammation.

OCIS codes: (170.3660) Light propagation in tissues; (170.6510) Spectroscopy, tissue diagnostics; (170.7230) Urology; (170.2655) Functional monitoring and imaging.

http://dx.doi.org/10.1364/OL.38.003566

Partial nephrectomies are performed for small renal masses to preserve maximal renal function. During this operation, the renal artery is clamped to prevent the entry of blood to the parenchyma of the kidney, thus minimizing blood loss and providing a clear field-of-view during surgery [1–3]. Unfortunately, clamping the renal artery causes renal ischemic reperfusion injury (IRI), which is characterized by kidney injury during an extended period of vessel clamping, and reperfusion after release of the clamps. This condition is known to cause permanent renal damage to the entire organ [1,2]. The lack of an accurate assessment of the severity and extent of renal injury during renal artery clamping is one of the major challenges all urologists face during a partial nephrectomy. A recent U.S. National Cancer Institute Surveillance Epidemiology and End Result (SEER) study showed that the percentage of patients developing any acute or chronic renal injury estimated to be 50.3% after partial nephrectomy, and 82.2% after radical nephrectomy [4]. In order to preserve maximal renal function by minimizing IRI, there is a critical need to study and understand the pathophysiology of IRI.

Currently, there is no mechanism of measuring real-time IRI during partial nephrectomy. The current method for determining IRI utilizes the patient's postoperative creatinine and estimated glomerular filtration rate (eGFR) to monitor for acute and chronic renal injury. Although these measurements may determine whether or not IRI has occurred after the procedure, they cannot be used during surgery. While hyperspectral imaging approaches have been used by other groups to monitor changes during partial nephrectomy [5–8], there are certain limitations. For one, conventional hyperspectral imaging is unable to decouple absorption from scattering in its measurements. Therefore, this imaging technique can only track relative changes in StO_2. Also, while StO_2 is an index for tissue metabolism, it has not yet been used directly to track IRI.

We present datasets obtained during arterial occlusion of three porcine kidney models using spatial frequency domain imaging (SFDI), a type of quantitative wide-field functional imaging that employs near-infrared (NIR) wavelengths. We demonstrate the ability of SFDI to produce absolute, quantitative values of oxygen saturation (StO_2) and the reduced scattering coefficient (μ_s') of the kidneys during renal arterial occlusion.

SFDI is a wide-field, noncontact imaging modality that measures spatially resolved absorption (μ_a) and reduced scattering (μ_s') parameters, thus allowing quantitative mapping of tissue optical properties [9–11]. Physically decoupling absorption from scattering is achieved by spatially modulating the light into a two-dimensional sinusoid that is projected onto the sample. Absorption is derived from the overall attenuation of the intensity of the diffusely reflected sinusoid from the sample, and scattering is derived from the degree to which the diffusely reflected sinusoid is blurred in space. By interrogating the sample at multiple wavelengths, we can compute absolute, quantitative measurements of chromphore concentrations such as oxy/deoxy-hemoglobin.

The SFDI instrumentation and data analysis have been described in detail previously [11,12]. A diagram of an SFDI system is shown in Fig. 1. Our SFDI instrument consists of three high-power LEDs with peak emission wavelengths of 658, 732, and 850 nm, with a power of <1 mW/cm^2 delivered to the surface of the tissue for each LED. The LEDs illuminate a digital micromirror device (DMD) (Texas Instruments, DMD Discovery 1100, Texas Instruments, Inc., Dallas, Texas). The DMD is used to spatially modulate the LED light, and project sinusoidal intensity patterns onto the kidney. In this set of experiments, we employed two spatial modulation

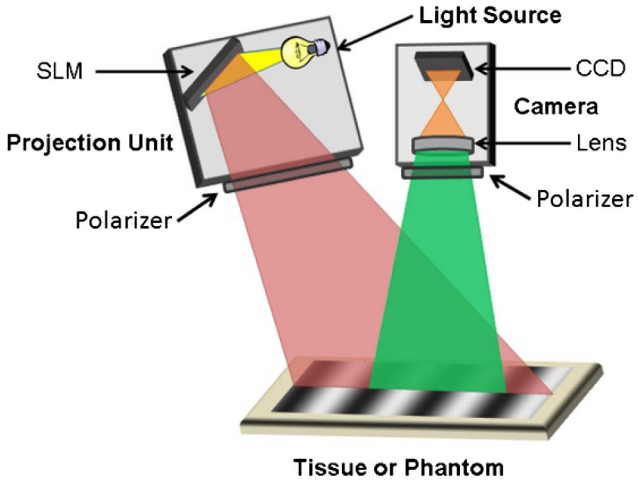

Fig. 1. Illustration of SFDI instrument. Patterned light is projected onto a sample using a light source coupled with a spatial light modulator (SLM) inside a projection unit. The diffusely reflected light is then coupled to a lens and detected by a CCD inside a camera.

frequencies (0 and 0.2 mm^{-1}). For each spatial frequency, the intensity pattern is projected at three distinct phases (0, 120, and 240 deg). The diffusely reflected light from the kidney is imaged onto a charge-coupled device (CCD). In order to correct for errors due to the curvature of the kidney, we also performed a profilometry calibration measurement on a sample with known optical properties [13]. To mitigate specular reflection, the projector and camera are equipped with crossed polarizers. In order to derive optical property maps, we fit the detected amplitude of the diffusely reflected light from the CCD at each pixel to a semi-infinite, homogeneous, Monte Carlo transport model, employing a fast lookup table approach using cubic spline interpolation on the diffuse reflectance data at two spatial frequencies (0 and 0.2 mm^{-1}). This method has been validated for separating absorption from scattering over a broad range of μ_s'/μ_a values spanning from ~0.5 to 300 [11]. Once the μ_s' and μ_a values were separated by SFDI, we calculated hemodynamic parameters from the scatter-corrected μ_a values assuming that oxy/deoxy-hemoglobin were the primary absorbers in the sample. From these values, we computed StO_2 from the percent ratio of oxy to total hemoglobin concentration. Data processing was executed using the MATLAB software suite (MATLAB and Statistics Toolbox Release 2010b, The MathWorks, Inc., Natick, Massachusetts).

The renal arterial occlusion procedure was performed on 30 kg, female Yorkshire pigs. The porcine kidney, ureter, and bladder have an anatomical location and function similar to those of the human urinary system. [14,15] We performed the procedure under general anesthesia after the pigs were intubated. Next, we positioned the pigs in the supine position, and a midline incision was made from the sternum to the pubis to enter the peritoneum. Then we mobilized the intraperitoneal organs away from the kidney to dissect the kidney in the retroperitoneum. We then isolated and dissected the renal artery to prepare for occlusion. Occlusion was performed using an occlusion balloon cuff (Docxs Biomedical, Ukiah, California) driven by a syringe pump (NE-1000, New Era, Farmingdale, New York), and an ultrasound flow probe (TS-420, Transonic System, Ithaca, New York) was placed downstream to monitor blood flow to the kidney. Our SFDI instrument was then positioned at the bedside next to the pig with the kidney exposed. The entire system was suspended above the kidney via an adjustable arm.

Image acquisition was performed over a period of 80 min in increments of approximately 2 min, with each data acquisition lasting approximately 10 s. We began acquiring images 10 min prior to arterial occlusion in order to establish a baseline for our StO_2 values. Arterial occlusion was established by rapidly inflating the occlusion balloon. Upon full expansion, blood flow was restricted to the kidney, and complete occlusion was confirmed by the flow meter throughout the study. We continued acquisition for a period of approximately 1 h while blood flow was restricted to the kidney, and also for an additional 10 min after reperfusion. In order to confirm that renal ischemia injury had occurred in our model, we also extracted tissue samples from the kidney at various time points. We employed an 18 gauge × 25 cm biopsy needle (Maxcore, Bard Medical, Covington, Georgia), and extracted two core samples from the superior pole kidney 3 just prior to occlusion, 5, 15, 30, 45, and 60 min during occlusion, and 10 min after reperfusion.

Our StO_2 and μ_s' (at 850 nm) datasets are shown in Fig. 2. We chose 850 nm for the scattering wavelength since light penetrates tissue deeper here than the other wavelengths available on our system (658 and 732 nm). For each dataset, we examined a region of interest (ROI) located in the top-right portion of the kidneys [Fig. 2(a)]. This ROI is 50 × 50 pixels, which corresponds to a field-of-view of roughly 1 × 1 cm. This ROI was chosen to avoid the effects of specular reflection in the center of the kidney, as well as errors due to curvature, which can be seen on the right edge of the kidney in the StO_2 and μ_s' maps.

Our StO_2 results for the three kidneys are shown in Fig. 2(b). Here we see an initial mean percentage of approximately 60%. Upon arterial occlusion, the mean StO_2 drops rapidly, reaching a value of approximately 20% within 5 min. Upon reperfusion, we see a rapid increase in mean StO_2 to 55%, recovering to near the baseline level of 60% within 10 min.

SFDI has the ability to decouple μ_s' from μ_a. Using this capability, which in terms of wide-field spectral imaging approaches is unique to SFDI, we are able to generate wide-field μ_s' maps, as well as scattering spectrum maps. In this analysis, all μ_s' values were taken from three ROIs, with additional ROIs located 1–1.5 cm to the left and right of the ROI shown in Fig 2(a). Figure 2(c) shows a plot of the average μ_s' for kidney 1 at the three ROIs, with the scattering spectrum embedded at the top at two time points. Here we see a decrease in the scattering power (SP), which is related to the scattering spectrum decay rate. From the beginning of occlusion (solid line) to the end of occlusion (dashed line), we see a decrease in SP from 1.05 to 0.88.

StO_2 values obtained prior to clamping could be informative in terms of the health of the kidney prior to clamping. As mentioned in the introduction, conventional hyperspectral imaging techniques are only able to monitor relative changes in StO_2. Since SFDI decouples

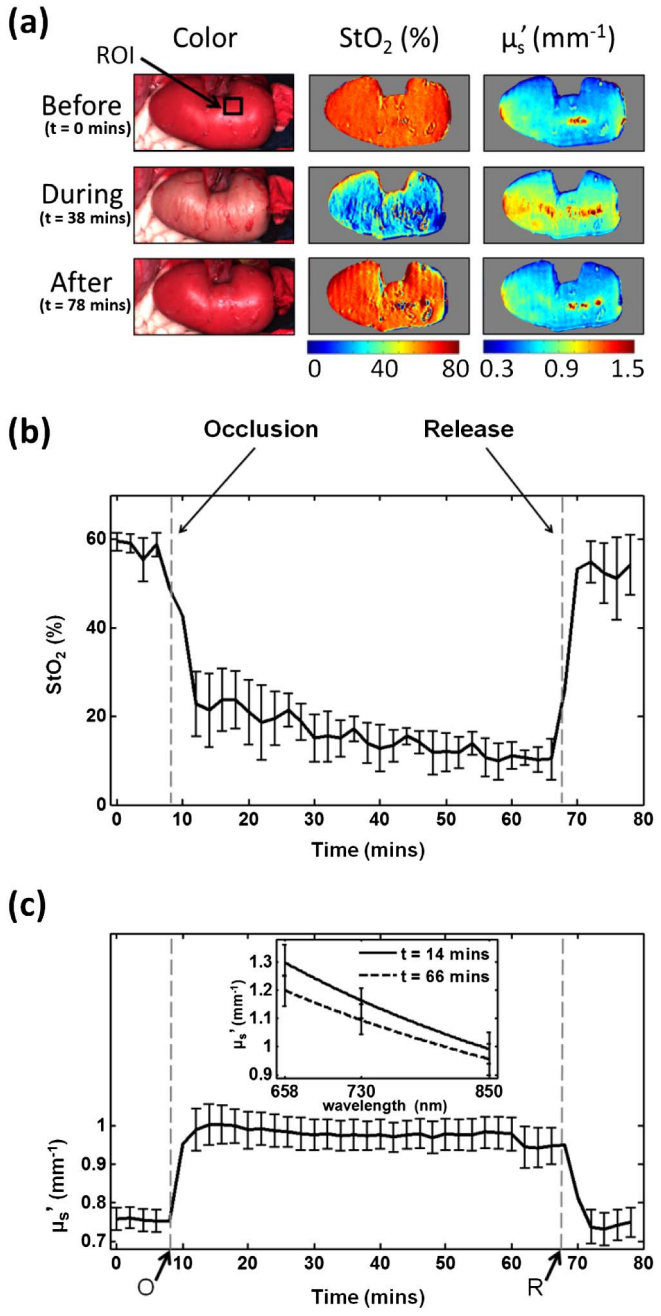

Fig. 2. (a) Color, StO_2, and μ_s' images of kidney 1 before, during, and after arterial occlusion. (b) Average StO_2 percentages for three kidneys before (<8 min), during (8–68 min), and after (>68 min) occlusion with standard error bars. (c) Plot of mean μ_s' (850 nm) of kidney 1 at three regions of interest with standard error bars, and μ_s' spectra 6 min after occlusion ($t = 14$), and 2 min before reperfusion ($t = 66$), with corresponding fits and standard error bars.

absorption from scattering, we are able to derive absolute values of StO_2 from our measurements. The health of the kidney prior to surgery may not be well characterized for a given patient. Therefore, baseline, absolute StO_2 measurements could be valuable in partial nephrectomy procedures. The mean StO_2 for the three kidneys was 58.9%, with a standard deviation of 3.7%. This value is lower than what has been reported previously using hyperspectral imaging on a similar model, which is around 70% [5–8]. Since we use NIR illumination, our mean interrogation depth is deeper than in previous techniques. Methods that employ visible light should produce higher StO_2 values since they interrogate more superficial, high-blood-flow regions of the renal cortex.

For each kidney, the amount of total hemoglobin increased during occlusion from beginning to end, with mean beginning and end values of approximately 250 and 350 μM, respectively. The increase in total hemoglobin during occlusion appeared to be due primarily to deoxyhemoglobin. In the absence of venous clamping, this is likely the result of retrograde flow of deoxygenated blood into the kidney.

In addition to establishing an accurate baseline for StO_2, it may be possible to monitor kidney function with SFDI during IRI. In particular, changes in μ_s' could potentially be used as a metric for oxidative stress and renal injury. The μ_s' values at 850 nm for kidneys 1, 2, and 3 increased upon occlusion (0.97, 0.72, and 0.52 mm^{-1} upon occlusion versus 0.73, 0.63, and 0.48 mm^{-1} for baseline values, respectively). Throughout the course of the occlusion, we saw a significant decrease in μ_s' in the three kidneys of 0.06, 0.05, and 0.09 mm^{-1}. A previous study using SFDI in an occlusion model also shows a decrease in μ_s'. [16] After reperfusion, the μ_s' values for each kidney returned to within 0.02 mm^{-1} of the baseline.

The scattering spectrum has been used previously to assess tissue scattering particle composition. In particular, the SP has been related to average scattering particle size [17,18]. In the case of Rayleigh scattering, SP is 4, and is roughly 1 in the case of Mie scattering. We observed a substantial decrease in the SP in each kidney during occlusion. In particular, from the beginning to end of occlusion, SP decreased from 1.05 to 0.88 in kidney 1 (16% decrease), 1.54 to 1.28 in kidney 2 (17% decrease), and 1.36 to 1.07 in kidney 3 (21% decrease). The decrease in SP during occlusion implies an increase in average scattering particle size. This is likely due to tissue changes such as edema that follow from occlusion and inflammation [19].

Epithelial cells in the kidney are known to succumb to injury and inflammation due to ischemia, which increases the permeability of the cell to its outside environment [19]. This structural alteration on the cellular level may correlate to the decrease in μ_s' and SP that we see in the three kidneys during occlusion. In order to examine this effect, we performed hematoxylin and eosin (H&E) and periodic acid-Schiff (PAS) stains on kidney biopsies. Figure 3 shows results from samples that were obtained during the experiment at specific time points. Here we demonstrate changes in the proximal tubules, which are known to be highly susceptible to the progression of IRI [19]. The sample shown in Fig. 3(a) was extracted just prior to occlusion, and shows normal proximal tubules. In Fig. 3(b), there is separation of the brush borders on the epithelial cells, and blurring of the cell borders, which occurred after 15 min of occlusion. In Fig. 3(c), after 60 min of occlusion, we see complete detachment of the epithelial cells from the basement membrane, as well as disappearance of the cell borders, which is indicative of an increase in cell permeability, and cellular edema. The average decrease in μ_s' and SP

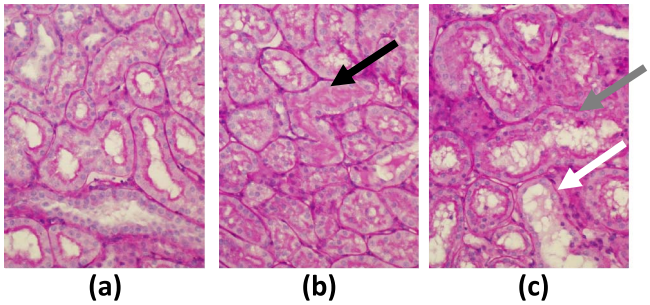

Fig. 3. Pathology slides (40×) showing the cross section of proximal tubules from kidney 3 (a) before occlusion (normal), (b) after 15 min of occlusion (separation of brush borders, shown by black arrow), and (c) after 1 h of occlusion (cell borders have disappeared, white arrow, and cells are detached from basement membrane, gray arrow).

in the three kidneys during occlusion could be associated with these structural changes.

In the future, we plan to correlate optical and physiological property changes with serum markers, such as creatinine and lactate, as well as with biomarkers of renal injury, such as neutrophil gelatinase-associated lipocalin (NGAL) and kidney injury molecule –1 (KIM-1) [19]. In addition, we will acquire data at 970 nm in order to quantify water content, an indicator of edema and inflammation. We expect that these studies will provide more detailed information on kidney viability and will move us closer toward developing a validated, real-time method for monitoring and predicting kidney IRI.

The authors gratefully acknowledge funding provided by the NIH NIBIB Biomedical Technology Research Center (grants LAMMP: P41EB015890, NIH NIBIB 1R03EB012194-01, and NIH NCATS UL1 TR000153), the Military Medical Photonics Program, AFOSR grant FA9550-08-1-0384, and the Beckman Foundation. K.P.N. was supported by NSF IGERT (grant 1144901), "Biophotonics across Energy, Space, and Time." B.J.T. and A.J.D. report patents owned by the University of California that are related to SFDI technology. B.J.T. and A.J.D. are cofounders of Modulated Imaging (MI), Inc., which has licensed SFDI from the University of California.

References

1. A. Nadu, N. Kitrey, Y. Mor, J. Golomb, and J. Ramon, Urology **66**, 279 (2005).
2. B. R. Lane and I. S. Gill, J. Urol. **177**, 70 (2007).
3. M. Topley, A. C. Novick, and J. E. Montie, J. Urol. **131**, 1050 (1984).
4. M. Sun, M. Bianchi, J. Hansen, Q. D. Trinh, F. Abdollah, Z. Tian, J. Sammon, S. F. Shariat, M. Graefen, F. Montorsi, P. Perrotte, and P. L. Karakiewicz, Eur. Urol. **62**, 696 (2012).
5. S. L. Best, A. Thapa, M. J. Holzer, N. Jackson, S. A. Mir, J. A. Cadeddu, and K. J. Zuzak, Urology **78**, 961 (2011).
6. M. S. Holzer, S. L. Best, N. Jackson, A. Thapa, G. V. Raj, J. A. Cadeddu, and K. J. Zuzak, J. Urol. **186**, 400 (2011).
7. C. R. Tracy, J. D. Terrell, R. P. Francis, E. F. Wehner, J. Smith, M. Litorja, D. L. Hawkins, M. S. Pearle, J. A. Cadeddu, and K. J. Zuzak, J. Endourol. **24**, 321 (2010).
8. Z. W. Liu, S. Faddegon, E. O. Olweny, S. L. Best, N. Jackson, G. V. Raj, K. J. Zuzak, and J. A. Cadeddu, J. Endourol. **27**, 470 (2013).
9. F. Bevilacqua, D. Cuccia, A. J. Durkin, and B. J. Tromberg, "Method and apparatus for performing quantitative analysis and imaging surfaces and subsurfaces of turbid media using spatially structured illumination," U.S. patent 6,958,815 (October 25, 2005).
10. D. J. Cuccia, F. Bevilacqua, A. J. Durkin, and B. J. Tromberg, Opt. Lett. **30**, 1354 (2005).
11. D. J. Cuccia, F. Bevilacqua, A. J. Durkin, and B. J. Tromberg, J. Biomed. Opt. **14**, 024012 (2009).
12. A. Mazhar, S. A. Sharif, D. J. Cuccia, S. J. Nelson, K. M. Kelly, and A. J. Durkin, Lasers Surg. Med. **44**, 611 (2012).
13. S. Gioux, A. Mazhar, D. J. Cuccia, A. J. Durkin, B. J. Tromberg, and J. V. Frangioni, J. Biomed. Opt. **14**, 034045 (2009).
14. D. Schwalb, M. Eshghi, J. Cord, R. Evans, E. Braga, I. Franco, J. Durso, and J. C. Addonizio, J. Endourol. **3**, 85 (1989).
15. F. J. Sampaio, M. A. Pereira-Sampaio, and L. A. Favorito, J. Endourol. **12**, 45 (1998).
16. D. Abookasis, C. C. Lay, M. S. Mathews, M. E. Linskey, R. D. Frostig, and B. J. Tromberg, J. Biomed. Opt. **14**, 024033 (2009).
17. J. Q. Nguyen, C. Crouzet, T. Mai, K. Riola, D. Uchitel, L. Liaw, N. Bernal, A. Ponticorvo, B. Choi, and A. J. Durkin, J. Biomed. Opt. **18**, 66010 (2013).
18. B. W. Pogue, S. Jiang, H. Dehghani, C. Kogel, S. Soho, S. Srinivasan, X. Song, T. D. Tosteson, S. P. Poplack, and K. D. Paulsen, J. Biomed. Opt. **9**, 541 (2004).
19. J. V. Bonventre and L. Yang, J. Clin. Invest. **121**, 4210 (2011).